The deficient *T* waves of tsunami earthquakes

Emile A. Okal,[1] Pierre-Jean Alasset,[2,*] Olivier Hyvernaud[2] and François Schindelé[3]

[1]*Department of Geological Sciences, Northwestern University, Evanston, IL 60208, USA. E-mail: emile@earth.northwestern.edu*
[2]*Laboratoire de Géophysique, Commissariat à l'Energie Atomique, Boîte Postale 640, F-98713 Papeete, Tahiti, French Polynesia*
[3]*Département Analyse et Surveillance de l'Environnement, Commissariat à l'Energie Atomique, BP 12, F-91680 Bruyères-le-Châtel, France*

SUMMARY

We develop an algorithm quantifying the energy flux of *T* phases recorded at island stations following major teleseismic events, which we further scale by the seismic moment M_0 of the earthquake, to define a *T*-phase efficiency, Γ. We apply this concept to a set of six recognized tsunami earthquakes, which generated tsunamis larger than expected from their conventional seismic waves. Through comparison with nearby reference events the *T* waves of which were recorded at the same sites, we find that the tsunami earthquakes exhibit a deficiency in Γ ranging from 1.5 to 2.5 orders of magnitude. This result settles a 50 yr old controversy on the possible correlation between *T*-wave generation and tsunami genesis. The deficient character of the *T* waves from tsunami earthquakes readily supports the proposed model of an exceedingly slow rupture velocity for this class of events, and the close examination of *T* wave trains supports the concept of a jerky rupture in at least two cases. The computation of Γ is straightforward in real time, and could become a valuable contribution to real-time tsunami warning in the far field.

Key words: Hydroacoustics; slow earthquakes; tsunamis; *T* waves.

1 INTRODUCTION AND BACKGROUND

This paper examines quantitatively the generation of *T* phases by the so-called 'tsunami earthquakes', characterized by larger tsunami generation than would be expected from their seismic waves, and in particular from their conventional magnitudes (Kanamori 1972; Newman & Okal 1998; Polet & Kanamori 2000). We recall that *T* phases are seismic waves recorded by seismometers, which have travelled the major part of the source-to-receiver path as acoustic waves channelled in the ocean water column by the SOFAR low-velocity waveguide (e.g. Ewing *et al.* 1946, 1952; Talandier & Okal 1998; Okal 2001a). We wish to stress here the difference between a 'tsunami earthquake', which is anomalously efficient in its tsunami generation, and a 'tsunamigenic earthquake', which is merely an earthquake that generated a detectable tsunami.

The question of the correlation, if any, between the generation of *T* waves and tsunamis by dislocation sources in the oceanic environment has been the subject of controversy ever since Ewing *et al.* (1950) suggested the use of *T* phases in tsunami warning. These authors' argument was that the generation of both kinds of waves would be favoured under strong coupling of the seismic source with the ocean column, which they attributed to the extreme shallowness of the seismic source. This model was disputed early on by Leet

*Now at: Institut de Physique du Globe, Université Louis Pasteur, 5 rue René Descartes, F-67084, Strasbourg Cedex, France.

(1951) and Wadati & Inouye (1953). We now understand, on the one hand, that under favourable geometries *T* waves can be generated by earthquakes of any depth (Northrop 1974; Okal & Talandier 1997, 1998; Okal 2001b), and, on the other hand, that the generation of strong far-field tsunami waves by earthquakes may be only moderately dependent on depth (Ward 1980; Okal 1988); both observations render Ewing *et al.*'s (1950) suggestion precarious.

Later, Okal & Talandier (1986) showed that the duration, rather than the amplitude, of teleseismic *T* waves could be correlated with the low-frequency seismic moment of the source, and hence with its tsunamigenic potential, an idea already sketched by Johnson (1970). More recently, Walker *et al.* (1992) and Walker & Bernard (1993) have quantified the power spectrum of *T* waves from a number of tsunamigenic earthquakes; while they concluded that the more tsunamigenic earthquakes did have generally stronger *T* waves, their data set predated the large tsunamis of the 1990s, and, in particular, the three 'tsunami earthquakes' of 1992 (Nicaragua), 1994 (Java) and 1996 (Chimbote, Peru).

The absence of a clear consensus regarding any correlation between the generation of tsunamis and *T* waves stems in large part from the extreme disparity in frequency between the two kinds of waves, the generation of tsunamis being controlled by the ultralow-frequency part of the source spectrum (typically below 2 mHz), and *T* waves propagating efficiently only if their wavelengths fit inside the width of the SOFAR channel, in practice if their frequency exceeds 2 Hz. While seismic scaling laws can be applied with perhaps surprising success to the vast majority of earthquakes (e.g. Tsuboi

416

1956; Geller 1976; Scholz 1982; Rundle 1989), it is evident that occasional variations in source parameters can significantly affect the relative behaviour of the seismic source at the two opposite ends of the frequency spectrum. Indeed, variations in stress drop, rupture velocity and local rigidity at the source have been proposed or demonstrated to explain the occurrence of tsunami earthquakes (Fukao 1979; Okal 1988; Kanamori & Kikuchi 1993; Polet & Kanamori 2000).

In the present study, we focus on tsunami earthquakes, and show conclusively that they are deficient *T*-wave generators, which we interpret as expressing a slower-than-normal release of elastic energy, resulting in a destructive interference at the high frequencies required for efficient propagation in the SOFAR channel.

2 METHODOLOGY

Our approach is essentially similar to that of Newman & Okal (1998). Building on the early work of Boatwright & Choy (1986), these authors developed an algorithm that measures the energy flux in the generalized *P* wave at a teleseismic receiver, and applies a distance correction (averaged over focal mechanism and depth), to obtain an estimate, E^E, of the seismic energy radiated at the source. While scaling laws predict a constant value of -4.90 for the parameter $\Theta = \log_{10} E^E / M_0$, Newman & Okal (1998) showed that tsunami earthquakes feature a systematic deficiency in Θ, which can reach 1–1.5 logarithmic units.

In the present paper, we similarly define the *T*-phase energy flux at a seismic receiver station as

$$\text{TPEF} = \rho \alpha \int_W [\dot{u}(t)]^2 \, dt, \tag{1}$$

where $\dot{u}(t)$ is the vertical ground velocity, W is an appropriate time window containing the *T* phase, ρ and α are the density and the *P*-wave velocity of the shallow receiver structure, respectively.

Following Newman & Okal (1998), we extend the time window W over the entire time axis, and then use Parseval's theorem to recast the computation of (1) into the frequency domain:

$$\text{TPEF} = \frac{\rho \alpha}{2\pi} \int_{-\infty}^{+\infty} \omega^2 |U(\omega)|^2 \, d\omega$$
$$\approx \frac{\rho \alpha}{\pi} \int_{\omega_{\min}}^{\omega_{\max}} \omega^2 |U(\omega)|^2 \, d\omega, \tag{2}$$

where $U(\omega)$ is the complex spectral amplitude of ground motion, and the integration bounds can be conveniently taken as $f_{\min} = 2$ Hz and $f_{\max} = 10$ Hz ($\omega = 2\pi f$), an expression of the low-frequency cut-off of the SOFAR channel and of the combined action as a low-pass filter of the post-conversion land path and of the response of the seismometer sensor. We further define the *T*-phase efficiency of the event at the particular station considered, Γ, by scaling TPEF to the seismic moment M_0 of the earthquake:

$$\Gamma = \frac{\text{TPEF}}{M_0}. \tag{3}$$

The rationale behind normalizing TPEF to M_0 stems from the observation that, under optimal conditions, teleseismic *T* phases recorded close enough to the receiving shore can be idealized as a simple translation along the SOFAR channel of the strong-motion time-series at the generating shore (Talandier & Okal 1998), band-passed filtered within the interval $\{f_{\min}, f_{\max}\}$. At the wavelengths considered (typically only a few hundred metres), the source-side conversion shore can be considered part of the body wave far field of

the earthquake, and thus, assuming that uniform scaling laws apply, the energy in the strong motion time-series, and eventually in the teleseismic *T* phase, will scale with earthquake size as M_0^2 / τ_0^3, itself proportional to M_0 (Vassiliou & Kanamori 1982; Newman & Okal 1998), where τ_0 is the duration of the source.

In the case of *T* phases, the exact amplitude of the ground motion (or velocity) at the receiver is controlled by a number of parameters, such as the topography at the converting slope and the velocity structure of the receiving shore, and their variations on a scale comparable to the wavelengths involved—typically 400 m or less for the acoustic wave. These cannot be known precisely, and for this reason, we do not seek to implement any corrections similar to those of Newman & Okal (1998) beyond the simple measurements defined in eqs (2) and (3). We verify easily that Γ has the dimension of an inverse surface (measured in m^{-2}); however, we cannot propose a simple physical explanation of Γ.

We thus restrict our approach to the comparison, *at the same receiver site*, of *T* waves recorded from earthquakes located in essentially the same epicentral areas, and for which the conversion processes at the receiver side, and underwater propagation effects, can reasonably be taken as equivalent. In practice, one such event will be a tsunami earthquake, the other(s) one or more regular shocks. This comparative approach has traditionally been used in previous studies of tsunami earthquakes (Kanamori 1972; Fukao 1979). Within this framework, we do not attempt to compare absolute *T*-phase energy flux values at different receiving sites (even located on the same island), nor at the same receiving site but for earthquakes in different seismic regions, since either of these situations could involve different regimes of conversion at the receiving shore. Rather, any difference in Γ between a tsunami earthquake and a reference event will express the efficiency of the process of seismic release, *at the source*, for generating *T*-wave energy into the ocean column.

Finally, we wish to emphasize that tsunami earthquakes remain extremely rare: only three such events are well documented in the seismic digital era, and a handful more over the previous 60 yr. In order to circumvent the resulting paucity of digital data, we develop in Appendix A a methodology allowing the extension of our measurements to analogue seismograms recorded on paper or film.

3 DATA SET: EARTHQUAKES AND STATIONS

In order to further explore the legitimacy of scaling TPEF to M_0, we first tested our concept on a data set of *T* phases recorded at the IRIS station RAR from seven earthquakes regrouped within a 250 km segment of the Central Chilean subduction zone, and the moments of which span three orders of magnitude (see Table 1). All earthquakes feature essentially the same focal mechanism, expressing the local interplate motion. Fig. 1 illustrates the general growth of TPEF with M_0; the average value of Γ is 2.5×10^{-25} m^{-2}, with a root-mean-square residual of only 0.34 logarithmic units. While a formal regression of the data set would yield a slightly lower slope of only 0.75 for $\log_{10}$TPEF versus $\log_{10} M_0$, the fit would be only marginally improved (dotted line in Fig. 1), and would be controlled by the largest earthquake in the data set, the great 1995 Antofagasta event, which indeed has been documented to feature a trend towards source slowness (Ruegg *et al.* 1996; Newman & Okal 1998). In conclusion, this experiment upholds the concept of a constant Γ for a regional cluster of events in which only the seismic moment is varied by more than three orders of magnitude.

Table 1. Earthquakes used in the present study.

Date D M (J) Y	Origin time (GMT)	Region	Epicentre (°N)	Epicentre (°E)	Magnitudes m_b	Magnitudes M_s	Moment(10^{27} dyn cm)	Θ Value	Θ Ref.	Remarks
11 Jul (192) 1993	13:36	Chile	−25.31	−70.56	6.2	6.1	0.101			
10 Dec (344) 1994	03:39	Chile	−23.50	−71.14	5.8	5.6	0.013			
30 Jul (211) 1995	05:11	Chile	−24.17	−70.74	6.6	7.3	12.1	−5.48	a	
30 Jul (211) 1995	21:05	Chile	−23.00	−70.74	5.6	5.7	0.020			
03 Jul (185) 1996	16:48	Chile	−23.24	−71.22	5.3	5.4	0.0077			
30 Jan (030) 1998	12:16	Chile	−23.02	−70.62	6.3	6.5	0.44			
08 Jan (008) 2000	11:59	Chile	−23.21	−70.66	5.8	5.9	0.041			
21 Feb (052) 1996	12:51	Chimbote, Peru	−9.69	−79.77	5.8	6.7	2.2	−6.00	b	Tsunami earthquake
12 Nov (317) 1996	16:59	Nazca, Peru	−15.05	−75.66	6.4	7.3	4.4	−5.00	b	
09 Feb (040) 1997	12:32	Nazca, Peru	−14.49	−76.28	5.7	5.8	0.017	−5.02	b	
11 May (131) 2002	10:43	Northcentral Peru	−10.53	−78.85	5.7	5.7	0.0035			
03 Apr (093) 1990	22:57	Nicaragua	11.42	−86.32	5.7	6.5	0.18	−5.26	b	
02 Sep (246) 1992	00:16	Nicaragua	11.75	−87.36	5.3	7.2	3.4	−6.30	b	Tsunami earthquake
05 Sep (249) 1992	21:48	Nicaragua	12.05	−87.39	5.3	6.0	0.011	−5.10	b	
20 Oct (293) 1963	00:53	Kuriles	44.87	150.32		7.0 PAS	7.5	−6.42	c	Tsunami earthquake
17 Jun (168) 1973	03:55	Nemuro-Oki	43.12	145.74	6.5	7.7	6.7			
10 Jun (161) 1975	13:47	Nemuro-Oki	43.18	147.36	5.8	7.0	0.8	−6.43	a	Tsunami earthquake
21 Jan (021) 1976	10:05	Kuriles	44.74	149.15	6.3	7.0	0.69			
09 Oct (282) 1994	07:55	Kuriles	43.89	147.95	6.5	7.1	0.94			Reference event
10 Oct (283) 1977	11:53	Tonga	−25.87	−175.37	6.6	7.2	1.02			
19 Dec (353) 1982	17:43	Tonga	−24.15	−175.97	5.9	7.7	2.0	−5.76	a	Tsunami earthquake
01 Apr (091) 1946	12:29	Aleutian	53.33	−163.00		7.4 PAS	60	−7.02	d	Tsunami earthquake
01 Apr (091) 1946	12:55	Aleutian	54.09	−163.14			0.8			

Events are listed chronologically within individual regions. Regions are listed in the order described in text.
References for values of Θ: (a) Newman & Okal (1998); (b) Okal & Newman (2001); (c) This study; (d) Okal & Lopez (2002).
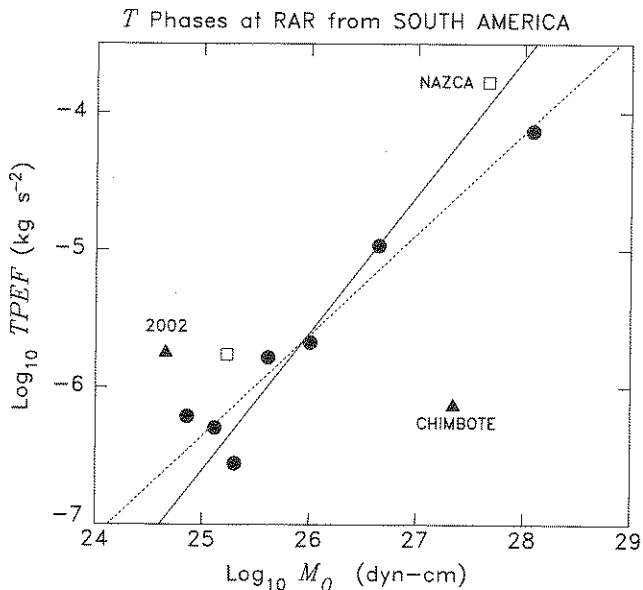

Figure 1. Solid circles show TPEF plotted against seismic moment for the seven Central Chilean earthquakes listed in Table 1. This figure upholds the model of a constant Γ, the best-fitting value of which, 2.5×10^{-25} m^{-2}, is shown by the solid line. The dotted line (with a slope of 0.75) is the best regression of the data set of seven points. The two open squares show the large 1996 Nazca event and its strong aftershock of 1997 January 30; note that they fit essentially the same trend of Γ (even though they belong to another geographical region along the coast of South America). The two triangles show the 1996 Chimbote tsunami earthquake, and the small 2002 event in its vicinity. Note the extreme T-wave deficiency of the Chimbote event, where the TPEF is deficient by two orders of magnitude, or approximately six times the scatter in the Chilean data.

We then focused on the most recent tsunami earthquakes, i.e. the three events in Nicaragua 1992 (Kikuchi & Kanamori 1995), Java 1994 (Tsuji *et al.* 1995) and Chimbote, Peru 1996 (Ihmlé *et al.* 1998), which motivated the detailed analysis of regional slowness by Okal & Newman (2001). Unfortunately, and because of sparse station coverage in the Indian Ocean at the time, we could find no adequate T-phase data for the 1994 Java tsunami earthquake. We add to the data set the events traditionally described as tsunami earthquakes in the literature but predating the establishment of the digital networks, namely the Aleutian earthquake of 1946 April 1 (Kanamori 1972), the Kuriles aftershock of 1963 October 20, the Nemuro-Oki earthquake of 1975 June 10 (Fukao 1979), and the 1982 Tonga shock reported by Talandier & Okal (1989) and later confirmed by Newman & Okal (1998) as a tsunami earthquake. Even older tsunami earthquakes, such as the Jalisco, Mexico aftershock of 1932 June 22, may be investigated in the future, should appropriate records become available.

For modern events, we use digital broad-band data, either from the IRIS and POSEIDON networks, or from the Polynesian Seismic Network (Réseau Sismique Polynésien, hereafter RSP). Continuous digital recording at the RSP started *ca.* 1994. Prior to that, analogue (paper) records are available. Fig. 2 shows a general map of the events and stations used in the present study, and Tables 1 and 2 provide all essential epicentral and receiver information.

4 RESULTS

4.1 Chimbote, Peru, 1996 February 21

This tsunami earthquake was followed within a few months (1996 November 12) by a regular event of comparable moment only
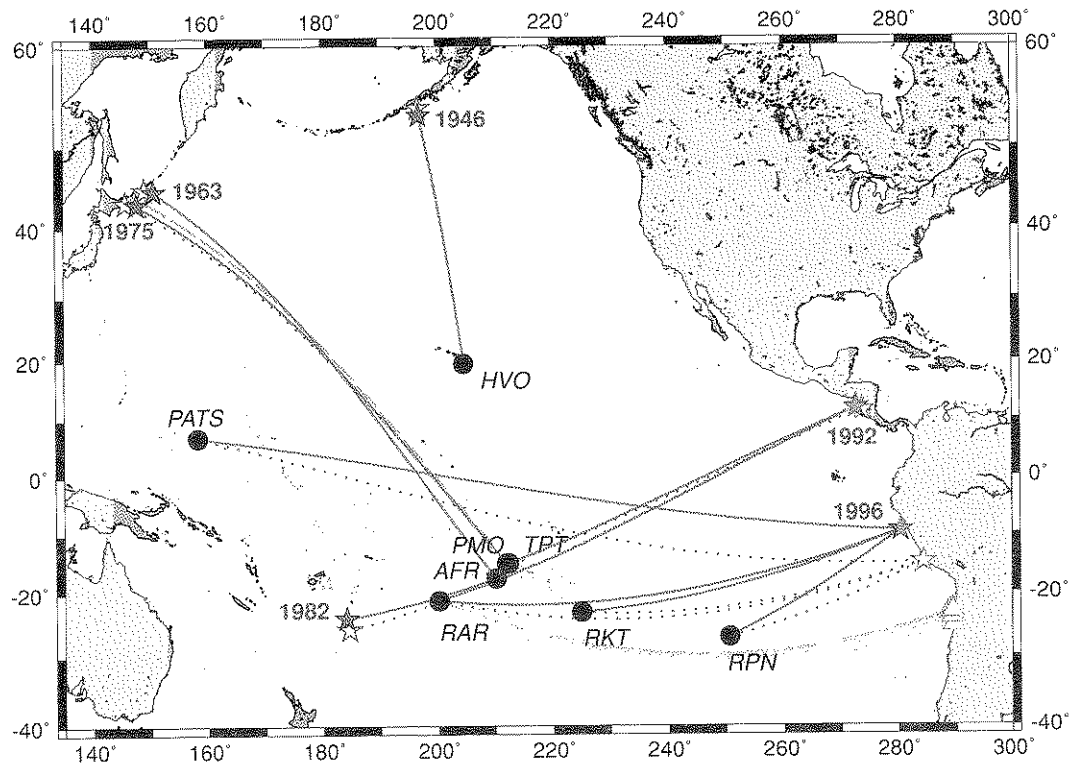
Figure 2. Map of events (stars) and stations (solid dots) used in this study (on the scale of this map, PMO and TPT cannot be resolved from each other). The solid stars represent the tsunami earthquakes (with year), the open ones the nearby reference events. The solid lines are the great circle paths from tsunami earthquakes analysed in this study; the dotted lines are the corresponding paths from the reference events. The grey open triangles and dotted lines are similarly the epicentres and paths for the reference data set of Central Chilean earthquakes. The dashed line is the path from the 1994 event to Rangiroa used in the Appendix for the evaluation of analogue record corrections.

Table 2. Characteristics of stations used in this study.

Code	Name	Coordinates		Network	Island	Chain	Geological setting (age if volcanic)	Distance to conversion shore	Type of recording (sampling rate if digital)
		(°N)	(°E)						
AFR	Afareaitu	−17.538	−149.778	RSP	Moorea	Society	Volcanic (2 Ma)	7 km	Analogue
PMO	Pomariorio	−15.017	−147.906	RSP	Rangiroa	Tuamotu	Atoll	50 m	Analogue; digital (50 Hz)
TPT	Tiputa	−14.984	−147.619	RSP	Rangiroa	Tuamotu	Atoll	50 m	Analogue; digital (50 Hz)
RKT	Rikitea	−23.118	−134.972	RSP	Mangareva	Gambier	Volcanic (6 Ma)	9 km	Digital (50 Hz)
RAR	Rarotonga	−21.210	−159.770	IRIS	Rarotonga	Cook	Volcanic (1.5 Ma)	2.5 km	Digital (20 Hz)
RPN	Rapa Nui	−27.127	−109.334	IRIS	Easter		Volcanic (1 Ma)	6–11 km[†]	Digital (20 Hz)
PATS	Pohnpei	6.837	158.315	POSEIDON	Pohnpei	Caroline	Volcanic (6 Ma)	3 km	Digital (10 Hz)
HVO	Uwekahuna	19.423	−155.293	HVO	Hawaii	Hawaii	Volcanic (0)	73 km	Analogue (smoked paper)

[†]Depending on azimuth (see text).

770 km further South. Newman & Okal (1998) documented a significant difference in the parameters Θ for the slow Chimbote tsunami earthquake ($\Theta = -6.00$), and the regular Nazca event ($\Theta = -5.00$). We were able to obtain T-phase records at four digital stations: RAR and RPN (IRIS), PATS (POSEIDON) and RKT (RSP).

Fig. 3 is a dramatic illustration of the difference in amplitude and waveshape between T phases for the two 1996 Peruvian earthquakes. The T phase of the Chimbote tsunami earthquake hardly emerges from the noise level at stations RAR and PATS, but the spectrogram techniques clearly extract the inversely dispersed T phase at RAR, approximately 135 s into the record (Fig. 4). Table 3 documents a systematic T-wave deficiency for the Chimbote event, relative to

Nazca, as expressed by the ratio of its values ($\Gamma_{Nazca}/\Gamma_{Chimbote}$) listed in the final column of the table.

For each station, the first set of measurements (hereafter the 'primary' set) is taken over a variable time window, as suggested by the spectrogram analysis (Fig. 4). Further measurements explore systematically the robustness of the results when integration parameters are varied: for example, we increase the time window of the Chimbote record, in order to match the Nazca one; this reduces only slightly the deficiency of the Chimbote T waves. We also test the influence of a lower f_{min} (1 Hz) in eq. (2). This is sufficient to significantly alter the deficiency of the tsunami earthquake, relative to the Nazca events, a probable contribution of background noise to the integral in eq. (2). On the other hand, reducing the frequency
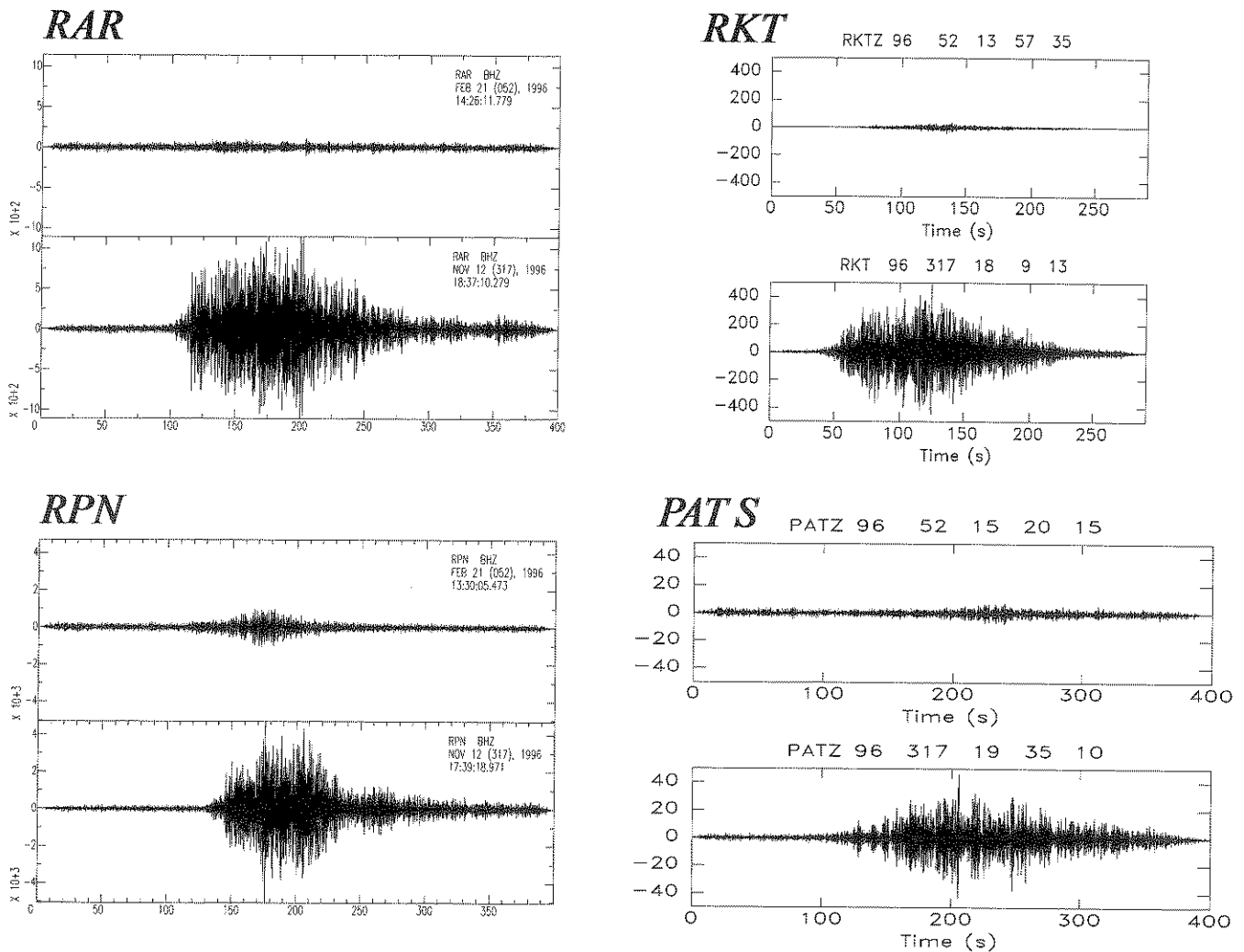
Figure 3. Comparison of T phases recorded at four teleseismic stations from the 1996 Chimbote and Nazca earthquakes. For each station, the two records are plotted on the same scale, after applying a high-pass filter ($f \geq 2$ Hz). The top trace is from the Chimbote tsunami earthquake (21 February), the bottom one from the regular Nazca event (12 November). Windows are 400 s long, except at Rikitea (290 s).

band (using $f_{max} = 5$ Hz) alters the results only marginally, as does the use of an artificially long window.

In general, results at RAR and RKT are very comparable, with deficiencies of the order of at least 100. However, at PATS and RPN, we obtain much lower values, 27 and 9.5, respectively, for the primary set. Regarding RPN, we note that Easter Island is a young shield volcano, with no coral reef, a geometry unfavourable to the acoustic $\rightarrow$ seismic conversion (Talandier & Okal 1998). Furthermore, the station is at the centre of the island, and being the closest station to the Peruvian coast, the difference in backazimuth is the largest (11°) in our data set; this implies conditions of conversion at the receiver, which may differ significantly for the two events, the great circles from the epicentres intersecting the shoreline in very different environments: a bay for Chimbote, and a long ridge for Nazca. In the case of PATS, we note that the Chimbote record is only marginally above the noise level in the frequency range available at PATS, where the Nyquist frequency is only 5 Hz, owing to the coarser sampling rate of the POSEIDON network.

In short, our results for the 1996 Peruvian events indicate that the most robust measurements are obtained at stations located on small volcanic edifices fringed by coral reefs, featuring improved

siting (RAR is in a borehole and the siting of the RSP stations was carefully optimized), and operating at an adequate sampling rate (at least 20 Hz). The integration domain should not be extended below 2 Hz. Results from the primary data sets at the best two stations then show that the Chimbote earthquake exhibits a deficiency in Γ exceeding two orders of magnitude.

As suggested by Okal and Newman's (2001) regional studies, it is probable that tsunami earthquakes have a tendency to occur in otherwise aseismic segments of the subduction boundary. As a result, and for lack of adequate seismic sources, we are generally unable to examine the T-wave deficiency of the Chimbote event relative to immediate neighbours, as we had done with the Central Chilean earthquakes in our preliminary study. However, we were able to expand our Peruvian study by using two additional, much smaller reference events. We first consider the largest aftershock (1997 February 9) of the regular Nazca event, for which the value of Γ is found to be consistent with that of the Nazca mainshock, which further upholds the concept of scaling TPEF to M_0 within a small geographic region. Incidentally, the agreement is also very good with values of Γ measured on the Central Chilean data set, which was not necessarily expected given the different orientation of the

RAR (Rarotonga) -- Vertical Broadband

21 FEB 1996 — CHIMBOTE, PERU — Tsunami Earthquake
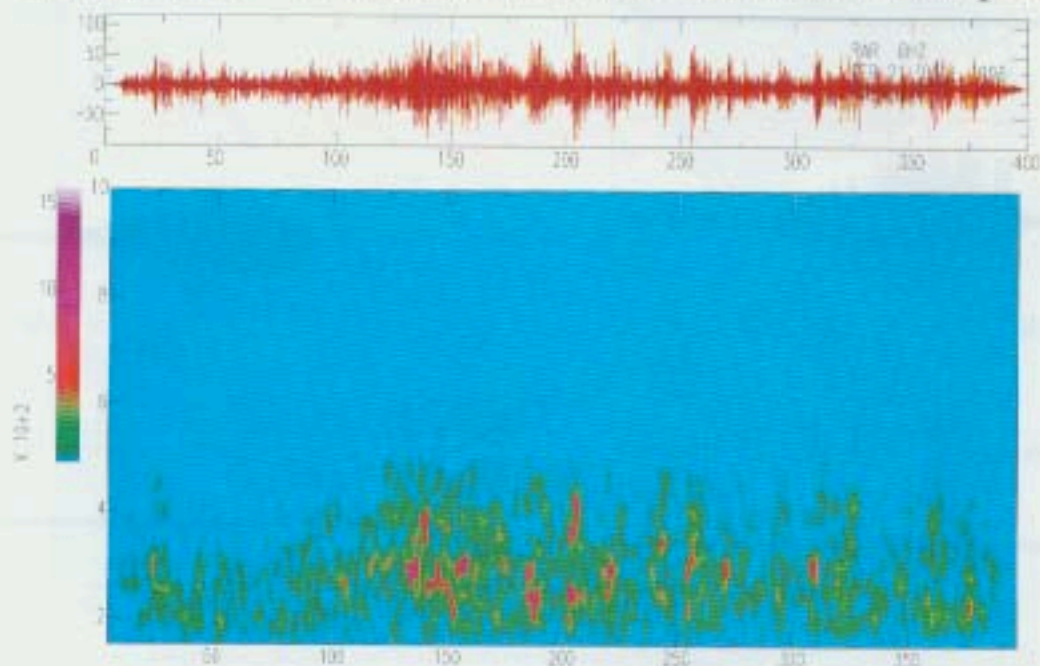
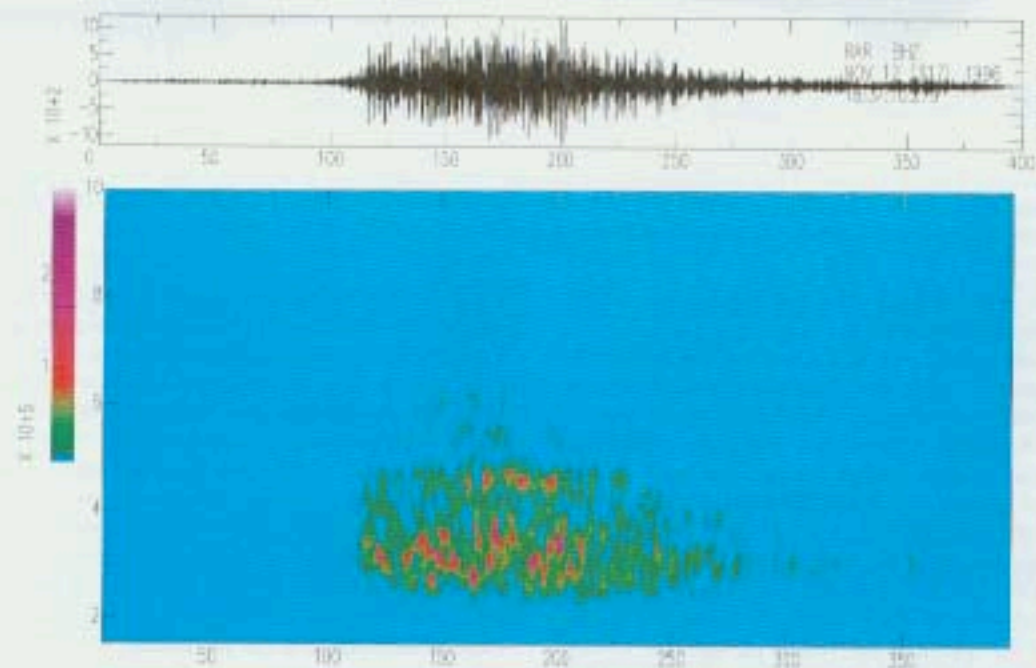## 12 NOV 1996 — NAZCA, PERU — Regular Earthquake

Figure 4. Comparison of spectrograms of *T* phases from the two 1996 Peruvian earthquakes, recorded at Rarotonga. The window of integration is 5 s long, and slides in units of 1 s. Note the much higher amplitude level (3×10^3 as opposed to 1.5×10^5) of the Nazca event, and the greater scatter in time and longer total duration of the Chimbote *T* phase, suggestive of a jerky rupture.

coastlines. Secondly, and by good fortune, a very small earthquake ($M_0 = 4.5 \times 10^{24}$ dyn cm) occurred recently (2002 May 11) only 135 km from the Chimbote epicentre. As detailed in Table 3, its TPEF is actually larger than that of the tsunami earthquake, despite

a moment more than 1000 times smaller. These results, included in Fig. 1, strongly support the concept of the source slowness of the 1996 tsunami earthquake as the origin of its deficient *T* waves, rather than a geographic process involving an unfavourable source

Table 3. Computation of Γ for the 1996 Chimbote, Peru tsunami earthquake.

Event	Distance (deg)	Backazimuth (deg)	Moment (10^{20} N m)	Duration of time window processed (s)	Frequency band		TPEF (kg s^{-2})	Γ (m^{-2})	Ratio to previous entry
					f_{min} (Hz)	f_{max} (Hz)			
Station: Rarotonga (RAR)									
96052 Chimbote	77.48	96	2.2	80	2	10	4.074×10^{-7}	1.85×10^{-27}	
96317 Nazca	79.29	102	4.6	188	2	10	1.666×10^{-4}	3.62×10^{-25}	196
96052 Chimbote	77.48	96	2.2	188	2	10	7.330×10^{-7}	3.33×10^{-27}	
96317 Nazca	79.29	102	4.6	188	2	10	1.666×10^{-4}	3.62×10^{-25}	109
96052 Chimbote	77.48	96	2.2	188	1	10	1.374×10^{-6}	6.25×10^{-27}	
96317 Nazca	79.29	102	4.6	188	1	10	1.672×10^{-4}	3.63×10^{-25}	58
96052 Chimbote	77.48	96	2.2	188	2	5	6.993×10^{-7}	3.18×10^{-27}	
96317 Nazca	79.29	102	4.6	188	2	5	1.479×10^{-4}	3.22×10^{-25}	101
96052 Chimbote	77.48	96	2.2	258	2	10	8.805×10^{-7}	4.00×10^{-27}	
96317 Nazca	79.29	102	4.6	258	2	10	1.671×10^{-4}	3.63×10^{-25}	91
96052 Chimbote	77.48	96	2.2	188	2	10	7.330×10^{-7}	3.33×10^{-27}	
02131 Northcentral Peru	77.85	97	0.0045	145	2	10	1.777×10^{-6}	3.95×10^{-24}	1185
96052 Chimbote	77.48	96	2.2	188	2	10	7.330×10^{-7}	3.33×10^{-27}	
97040 Nazca	78.91	101	0.017	100	2	10	1.73×10^{-6}	1.02×10^{-24}	305
Station: Rikitea (RKT)									
96052 Chimbote	53.80	86	2.2	103	2	10	2.614×10^{-6}	1.19×10^{-26}	
96317 Nazca	76.56	93	4.6	192	2	10	7.133×10^{-4}	1.55×10^{-24}	130
96052 Chimbote	53.80	86	2.2	192	2	10	2.918×10^{-6}	1.33×10^{-26}	
96317 Nazca	76.56	93	4.6	192	2	10	7.133×10^{-4}	1.55×10^{-24}	117
96052 Chimbote	53.80	86	2.2	192	1	10	5.675×10^{-6}	2.58×10^{-26}	
96317 Nazca	76.56	93	4.6	192	1	10	7.146×10^{-4}	1.55×10^{-24}	60
96052 Chimbote	53.80	86	2.2	192	2	5	2.730×10^{-6}	1.24×10^{-26}	
96317 Nazca	76.56	93	4.6	192	2	5	6.096×10^{-4}	1.33×10^{-24}	107
Station: Pohnpei (PATS)									
96052 Chimbote	122.68	97	2.2	152	2	5	3.855×10^{-8}	1.75×10^{-28}	
96317 Nazca	126.48	103	4.6	229	2	5	2.212×10^{-6}	4.81×10^{-27}	27
96052 Chimbote	122.68	97	2.2	229	2	5	7.539×10^{-8}	3.43×10^{-28}	
96317 Nazca	126.48	103	4.6	229	2	5	2.212×10^{-6}	4.81×10^{-27}	14
96052 Chimbote	122.68	97	2.2	229	1	5	3.326×10^{-6}	1.51×10^{-26}	
96317 Nazca	126.48	103	4.6	229	1	5	3.572×10^{-6}	7.76×10^{-27}	0.5
96052 Chimbote	122.68	97	2.2	229	3	5	1.032×10^{-8}	4.69×10^{-29}	
96317 Nazca	126.48	103	4.6	229	3	5	4.985×10^{-7}	1.08×10^{-27}	23
Station: Rapa Nui (RPN)									
96052 Chimbote	33.87	65	2.2	144	2	10	1.724×10^{-4}	7.83×10^{-25}	
96317 Nazca	33.54	76	4.6	270	2	10	3.424×10^{-3}	7.44×10^{-24}	9.5
96052 Chimbote	33.87	65	2.2	270	2	10	1.838×10^{-3}	8.35×10^{-25}	
96317 Nazca	33.54	76	4.6	270	2	10	3.424×10^{-3}	7.44×10^{-24}	8.9
96052 Chimbote	33.87	65	2.2	270	1	10	2.056×10^{-3}	9.35×10^{-25}	
96317 Nazca	33.54	76	4.6	270	1	10	3.440×10^{-3}	7.48×10^{-24}	8.9
96052 Chimbote	33.87	65	2.2	270	3	10	9.043×10^{-5}	4.11×10^{-25}	
96317 Nazca	33.54	76	4.6	270	3	10	2.732×10^{-3}	5.94×10^{-24}	14

geometry, e.g. blockage. The bottom line of the full Peruvian data set presented in Table 3 is that the deficiency of Γ for the Chimbote earthquake is consistently two orders of magnitude with respect to three neighbouring earthquakes (large and small), i.e. six times the scatter found across three orders of M_0 for a homogeneous data set of subduction earthquakes in a part of the South American subduction zone featuring a more sustained level of seismicity.

4.2 Nicaragua, 1992 September 2

Only paper records are available at the RSP for this event. The record at TPT is characterized by a long T phase, lasting approximately 4 min, but remaining on scale on the high-gain short-period channel (with a gain of 125 000 at 1 Hz). We use as a reference event the smaller shock of 1990 April 3, only 120 km away, and showing

no more than a slight trend towards slowness ($\Theta = -5.26$, Okal & Newman 2001). Both great circle paths to TPT intersect the atolls of Ahe and Manihi, 120 km out of TPT, and the energy fluxes at TPT could be affected. However, the relative value of the fluxes can reasonably be assumed to remain meaningful. In addition, and because both time-series were digitized from paper records, the values of Γ can be compared directly without the need for the empirical corrections developed in Appendix A. Fig. 5 shows the time-series of the T phases after digitization. As detailed in Table 4, the 1992 tsunami earthquake is found to be deficient by a factor of 115 with respect to its 1990 counterpart.

The only available IRIS record of a T phase from the 1992 earthquake is once again at RAR, with the great circle crossing both the Tuamotu archipelago (bisecting the large atoll of Fakarava) and the Island of Tahiti. Thus, the T phase recorded at RAR is probably diffracted around atolls of the Tuamotu group, and possibly
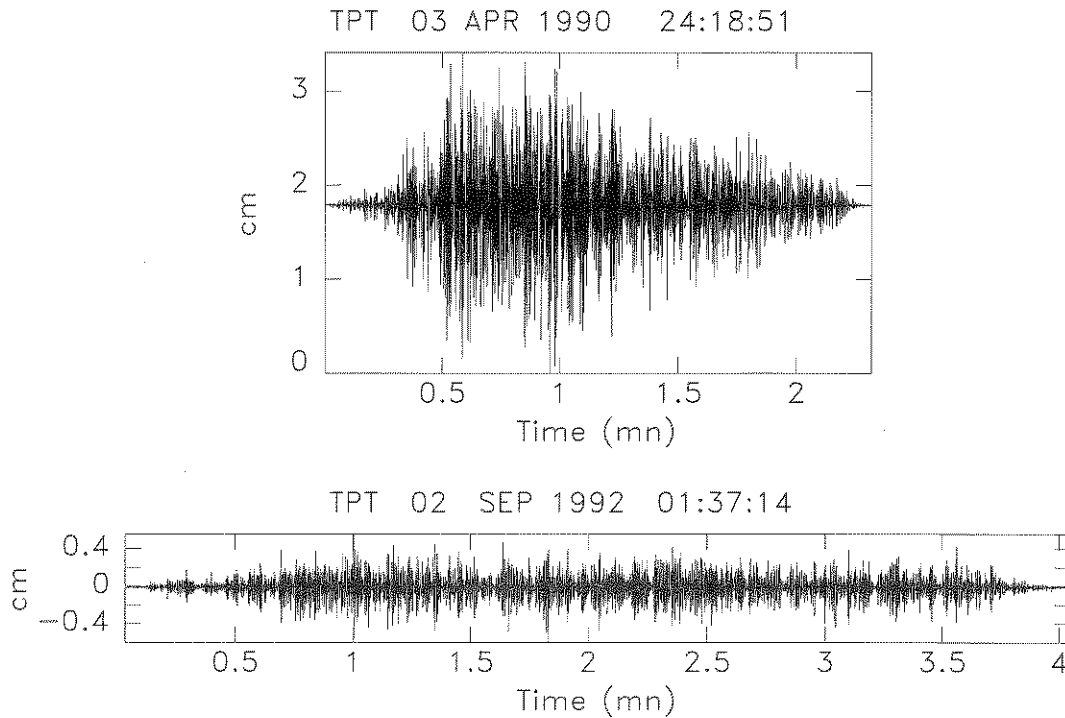
Figure 5. *T*-phase seismograms at TPT for the Nicaraguan earthquakes. Top: 1990 reference event; bottom: 1992 tsunami earthquake, plotted on common horizontal and vertical scales to allow a direct comparison. The records have been hand-digitized to a 0.05 s sampling, and high-pass filtered at 2 Hz. Note that the 1992 *T* phase does not feature the spindle shape characteristic of simple sources, but rather exhibits a long and discontinuous waveshape with no clear maximum.

Table 4. Results for the 1992 Nicaraguan tsunami earthquake.

Event	Distance	Backazimuth	Moment	Duration of time window processed (s)	Frequency band		TPEF	Γ	Ratio to previous entry
	(deg)	(deg)	$(10^{20}$ N m)		f_{min} (Hz)	f_{max} (Hz)	$(kg\ s^{-2})$	(m^{-2})	
				Station: Tiputa (TPT)					
92246 Nicaragua (paper)	65.37	69	3.4	241	2	5	3.12×10^{-6}	9.17×10^{-27}	
90093 Nicaragua (paper)	66.19	70	0.18	139	2	5	1.88×10^{-5}	1.05×10^{-24}	115
				Station: Rarotonga (RAR)					
92246 Nicaragua	77.67	73	3.4	230	2	5	3.29×10^{-6}	9.67×10^{-27}	
92249 Nicaragua	77.84	73	0.011	150	2	5	3.18×10^{-7}	2.89×10^{-25}	30
92246 Nicaragua	77.67	73	3.4	100	2	5	1.55×10^{-6}	4.55×10^{-27}	
92249 Nicaragua (Trimmed)	77.84	73	0.011	100	2	5	2.00×10^{-7}	1.82×10^{-25}	40

tunnelled through Tahiti, where the Taravao isthmus is only 2 km wide at its narrowest point. We use as a reference event the large aftershock of 1992 September 5 ($M_0 = 1.1 \times 10^{25}$ dyn cm) which Okal & Newman (2001) determined to have a regular slowness ($\Theta = -5.10$). It took place on the northern edge of the rupture area of the mainshock, and thus the two sources can be considered to be geographically identical, and their parameters Γ can be directly compared. We could not detect *T* phases above the noise level from any of the other aftershocks. Unfortunately, a glitch is present in the RAR record of the aftershock, 20 s before the arrival of the *T* wave. We therefore process both a 150 s window of the record including the glitch, and a shorter (100 s) window starting immediately after the glitch. The latter is compared with a window of similar length for the tsunami earthquake, selected to maximize the signal. As detailed in Table 4, the deficiency in Γ for the tsunami earthquake is found to be 30 on the full record and 40 on the trimmed one.

Unfortunately, we could not find a larger data set of reference events against which to further assess the *T*-wave deficiency of the

Nicaragua tsunami earthquake. In addition to the paucity of subduction activity in its vicinity (Okal & Newman 2001), we note that the only consistent digital station at the time (1992) was RAR, which is masked by the Tuamotu Islands from many epicentral areas in Central America. Nevertheless, we present strong evidence that the 1992 tsunami earthquake was significantly deficient with respect to at least two nearby shocks, including a large aftershock.

4.3 Nemuro-Oki, 1975 June 10

This event was recognized as a tsunami earthquake by Fukao (1979), who interpreted it as a relatively steeply dipping fault through the weak accretionary prism overlying the sinking slab, and resulting from stress transfer following the Nemuro-Oki interplate shock of 1973 June 17. The 1973 and 1975 events raised local tsunamis of comparable amplitudes, despite significantly different moments (6.7×10^{27} and 8×10^{26} dyn cm, respectively; Shimazaki 1975;
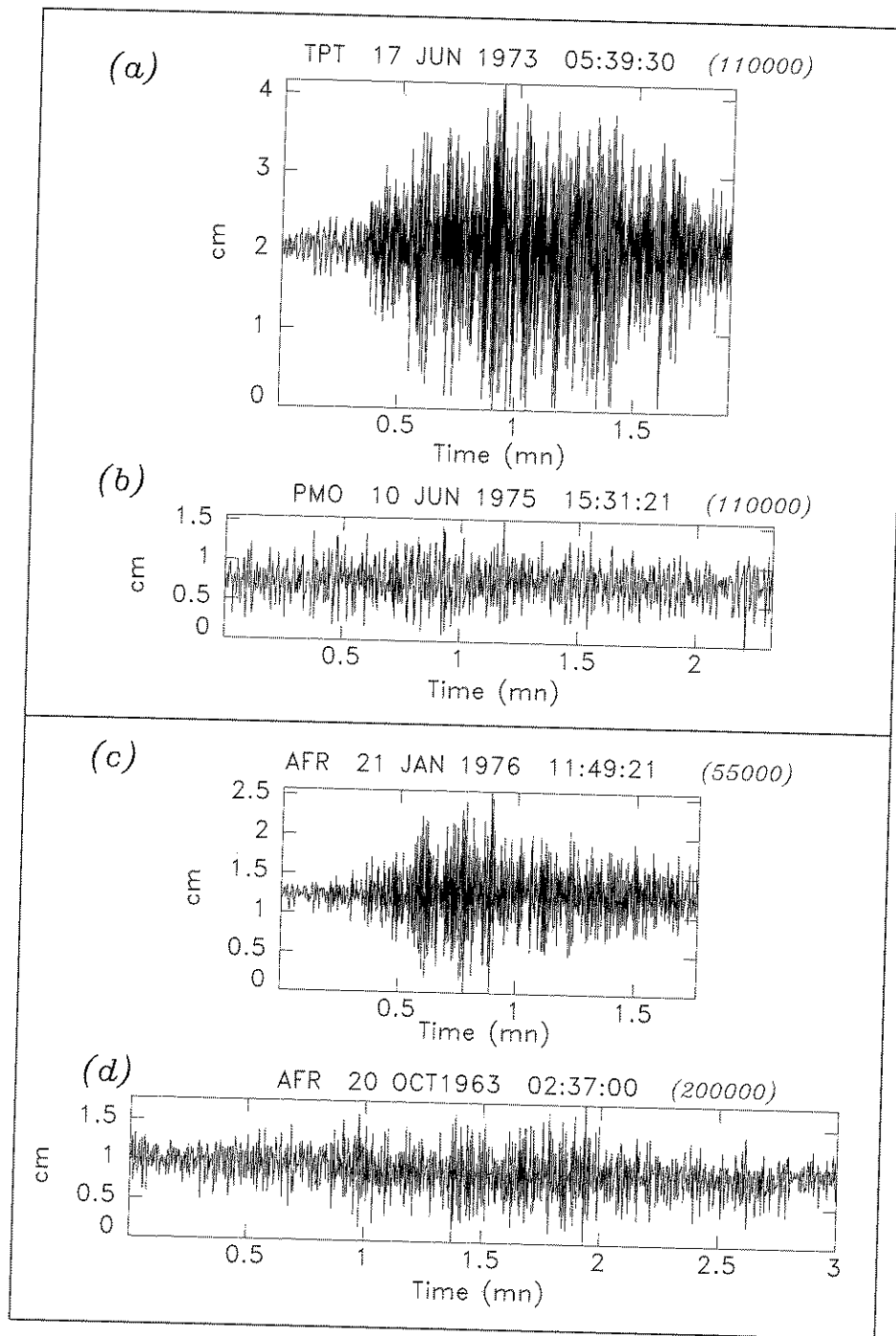
Figure 6. Top box: comparison of T phases from the Nemuro-Oki 1973 event (a) and 1975 tsunami earthquake (b). Bottom box: comparison of T phases recorded at AFR from the 1963 Kuriles tsunami earthquake (d) and the much smaller 1976 reference event (c). All time and amplitude scales are common on the four frames. Note, however, that the gains of the instruments (given in italics on each frame at $f = 1$ Hz) vary between frames. In both cases, the tsunami earthquake is characterized by a smaller amplitude, a large scatter of energy with time and the absence of a spindle-shaped wave train.

Fukao 1979). We confirmed the slow character of the 1975 event by applying Okal & Newman's (2001) algorithm to the Benioff 1—90 record at Pasadena ($\Theta = -6.43$).

As shown in Fig. 6, T waves from the 1975 event were recorded only at PMO (Pomariorio) on the northwestern shore of Rangiroa, with a mediocre amplitude on the high-gain short-period channel (in 1975, the RSP featured only paper records). They were not recorded above the noise level elsewhere in Polynesia. In contrast, the same

PMO channel was also totally saturated by the T phase of the 1973 Nemuro-Oki earthquake. We could find no readable record of the 1975 T waves at Pacific WWSSN stations, while the 1973 event was well recorded at Afiamalu, Western Samoa.

In order to quantify the T-wave deficiency of the 1975 tsunami earthquake, we digitized its lone record at PMO. As reference records, we use the 1994 digital record at PMO, and the 1973 paper record at TPT (Tiputa), 18 km further east along the northern coast

Table 5. Results for the 1975 Kuriles tsunami earthquake.

Event	Distance (deg)	Backazimuth (deg)	Moment (10^{20} N m)	Duration of time window processed (s)	Frequency band f_{min} (Hz)	f_{max} (Hz)	TPEF (kg s^{-2})	Γ (m^{-2})	Ratio to 1975 PMO (digital estimate)
				Station: Pomariorio (PMO)					
75161 Kuriles (paper)	82.52	318	0.8	139	2	5	2.17×10^{-6}		
75161 Kuriles (est. dig.)	82.52	318	0.8	139	2	5	5.79×10^{-6}	7.23×10^{-26}	
94282 Kuriles (dig.)	82.84	319	0.94	150	2	5	1.94×10^{-4}	2.07×10^{-24}	29
				Station: Tiputa (TPT)					
73168 Kuriles (paper)	84.04	318	6.7	115	2	5	4.91×10^{-5}		
73168 Kuriles (est. dig.)	84.04	318	6.7	115	2	5	1.31×10^{-4}		
73168 Kuriles (extrap. PMO)	84.04	318	6.7	115	2	5	3.35×10^{-3}	5.01×10^{-24}	69

Table 6. Results for the 1963 Kuriles tsunami earthquake.

Event	Distance (deg)	Backazimuth (deg)	Moment (10^{20} N m)	Duration of time window processed (s)	Frequency band f_{min} (Hz)	f_{max} (Hz)	TPEF (kg s^{-2})	Γ (m^{-2})	Ratio to previous entry
				Station: Afareaitu (AFR)					
63293 Kuriles (paper)	82.33	322	7.5	180	2	5	1.36×10^{-6}	1.81×10^{-27}	
76021 Kuriles (paper)	82.74	321	0.69	106	2	5	3.76×10^{-5}	5.45×10^{-25}	301

of Rangiroa (see the map in Fig. A2). Appendix A discusses the corrections used to alleviate the impossibility of a direct comparison at PMO. We find a raw flux TPEF$_{paper}$ = 2.17×10^{-6} kg s^{-2} in the frequency band 2–5 Hz, leading to $\Gamma = 7.23 \times 10^{-26}$ m^{-2}, using the empirical corrections determined in Appendix A. When compared with $\Gamma = 2.07 \times 10^{-24}$ m^{-2} for the 1994 Kuriles event, the deficiency reaches a factor of 29. For the 1973 earthquake, we compute a raw flux TPEF$_{paper}$ = 4.91×10^{-5} kg s^{-2} from the paper record at TPT, correct it to a digital estimate TPEF$_{dig}$ = 1.31×10^{-4} kg s^{-2}, and extrapolate it to 3.35×10^{-3} kg s^{-2} at PMO, finally yielding $\Gamma = 5.01 \times 10^{-24}$ m^{-2}. As detailed in Table 5, the deficiency in Γ for the 1975 event relative to the 1973 Nemuro-Oki earthquake reaches a factor of 69.

Routine observation of T phases from events comparable in location and seismic moment to the 1975 tsunami earthquake confirms that their T phases generally saturated the high-gain short-period channel at PMO; in addition to the reference event of 1994 October 9 (07:55; see Appendix A), examples would include the shocks of 1978 March 23 (00:31), 1980 February 23 (05:51) and 1984 March 24 (09:44). In conclusion, the 1975 tsunami earthquake shares with the previous two cases studied a systematic deficiency of its T waves relative to its immediate neighbours.

4.4 Kuriles, 1963 October 20

This event, the main aftershock of the great earthquake of 1963 October 13, is another classic example of a tsunami earthquake: as detailed by Fukao (1979), it features deficient high-frequency P waves, and enhanced ultra-long period surface waves, relative for example to the main foreshock (12 October), which had a comparable 20 s magnitude ($M_s = 6\frac{3}{4}$–7); it also generated a local tsunami only ~2.5 times smaller than that of the mainshock. Pelayo (1990) proposed a moment of 6×10^{27} dyn cm; our own mantle magnitude measurements ($M_m = 7.62$; $M_c = 7.88$ in Pelayo's 1990 focal geometry) suggest 7.5×10^{27} dyn cm, in agreement with Fukao's (1979) observation of an ultra-long period spectral ratio of approximately 1/11 relative to the mainshock ($M_0 = 7.5 \times 10^{28}$ dyn cm; Kanamori 1970), and with Ben-Menahem & Rosenman's

(1972) similar ratio of 6/70 for their relative 'potencies'. We confirm here the very slow character of the aftershock by applying Okal & Newman's (2001) algorithm to the Benioff 1–90 record at Pasadena ($\Theta = -6.42$).

The only usable (unclipped) T-wave record available for processing is that at Afareaitu (AFR), on the island of Moorea. We were unable to detect T waves above the noise level on the WWSSN records at Kipapa, Oahu, nor at Haleakala, Maui, a station that prominently recorded those of the mainshock and of other, smaller, aftershocks. As a reference event, we use the smaller nearby event of 1976 January 21 for which a CMT solution ($M_0 = 6.9 \times 10^{26}$ dyn cm) is available (Ekström & Nettles 1997). Fig. 6 clearly shows the weak amplitude and long duration of the T waves of the 1963 aftershock, and as detailed in Table 6, the deficiency in Γ for the tsunami earthquake, relative to the 1976 event, reaches 300.

4.5 Other records

We study here two additional events featuring a strong deficiency of T waves, but the records of which could not be fully processed and an estimate of Γ obtained.

4.5.1 Tonga, 1982 December 19

This event ($M_0 = 2 \times 10^{27}$ dyn cm) was recognized as a tsunami earthquake by Talandier & Okal (1989), and Newman & Okal (1998) documented a substantial slowness anomaly ($\Theta = -5.76$). Fig. 7 (bottom trace) shows that its T phase at AFR is relatively weak, with a peak-to-peak amplitude of 1.3 cm on the high-gain channel (gain of 62 500 at 1 Hz). It can be compared with the nearby shock of 1977 October 10 (11:53 GMT), which saturated the same channel operating at the same gain for 1.5 min, despite a smaller moment of only 1.02×10^{27} dyn cm. We could not find records of T phases of the 1982 event at other Pacific sites. For lack of an adequate digitally recorded or unsaturated analogue reference wave train, this study must remain qualitative, but Fig. 7 leaves no doubt that the slow 1982 tsunami earthquake exhibits a strong T-wave deficiency at AFR.
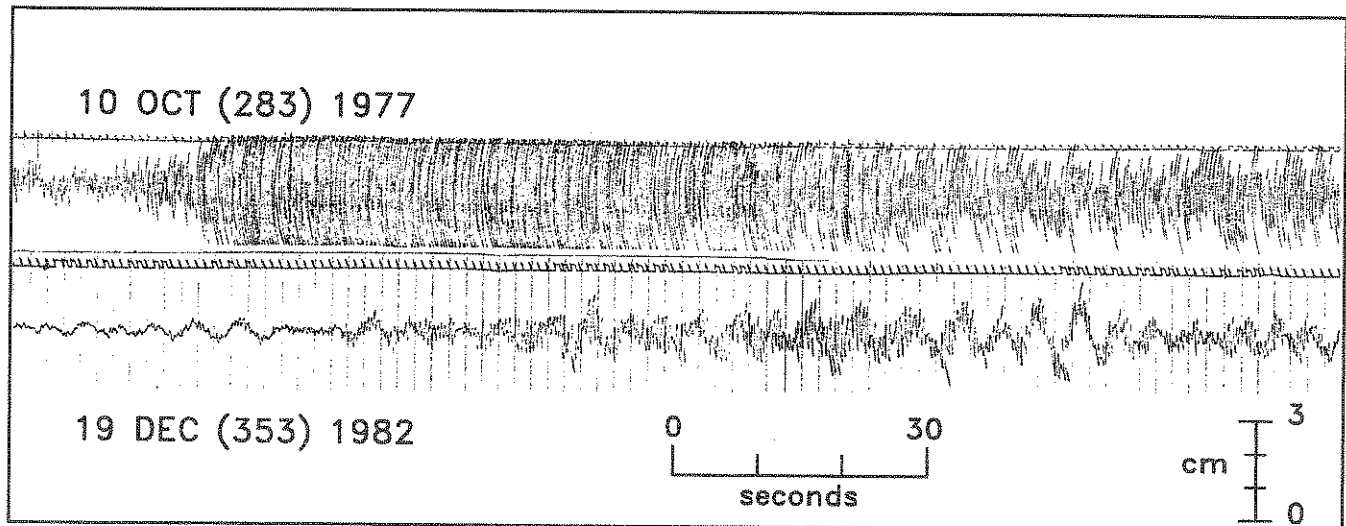
Figure 7. Comparison of T phases recorded at Afareaitu (AFR) for the tsunami earthquake of 1982 December 19 in South Tonga (bottom), and the reference event of 1977 October 10, only 200 km away (top). Tick marks are in seconds, and the scale at right gives the amplitude of the signal on the original paper records operating at a gain of 62 500 at 1 Hz. The 6 s oscillations prominent on the 1982 record are an example of strong sea swell recorded by the station, located only 2 km from the coral reef surrounding the island of Moorea.

4.5.2 Aleutian Islands, 1946 April 1

The Aleutian earthquake of 1946 April 1 remains a challenge to the scientific community: despite a relatively low conventional magnitude ($M_{PAS} = 7.4$), its tsunami was catastrophic both in the near field, where a run-up of 42 m eradicated the Scotch Cap lighthouse, and in the far field where it took 159 lives in Hawaii, caused significant damage and two further deaths in the Marquesas, and even some destruction in Antarctica (Okal *et al.* 2002; Plafker *et al.* 2002). Indeed, it was one of two events used by Kanamori (1972) in his landmark study defining tsunami earthquakes.

While the 1946 earthquake has long been documented as exceedingly slow (Kanamori 1972; Pelayo 1990; Okal & Lopez 2002), the possible contribution of a substantial underwater landslide to the source of the tsunami remains the subject of controversy (Kanamori 1985; Johnson & Satake 1997; Plafker *et al.* 2002). In this context the analysis of any T-phase record from the 1946 event is bound to be highly valuable.

We recently gained access to a recording of the 1946 Aleutian earthquake on the E–W Bosch–Omori seismometer at the Hawaii Volcano Observatory (HVO), of which a section is reproduced in Fig. 8. A high-frequency wave train is recognizable, barely emerging from the noise level, but clearly featuring the general characteristics (frequency, duration) of a T phase. This signal was examined by Walker & Okubo (1994), who concluded that the 1946 event had indeed generated a detectable T phase at HVO under what amounts to unfavourable conditions (poor magnification of the historical seismograph and an extended land path of at least 70 km at the receiver), thus lending support to Walker & Bernard's (1993) proposed association of strong T phases with tsunami genesis.

However, careful examination of the timing of the HVO record indicates that this T phase cannot have emanated from the Aleutian mainshock. While there could remain some uncertainty as to a possible clock correction, the arrival of the T wave train can be timed precisely *relative* to other seismic phases recorded on the same seismogram from the mainshock and its aftershocks, the timing of which can be assessed to a precision of a few seconds, based on the relocations of those events (Okal & Lopez 2002). The result is that the maximum of the T phase is recorded at HVO approximately 58.5 min after the S wave from the mainshock (the P wave is emergent and very difficult to interpret) and 31.5 min after the S wave from the main aftershock, which translates into an arrival time of 13:40 GMT (03:10 local time in 1946), or 71 min after the mainshock origin time (12:29:01 GMT). This is irreconcilable with a propagation time estimated at 42.3 min on the basis of the models of Levitus *et al.* (1994) for hydroacoustic propagation and Talandier & Okal (1998) for acoustic-to-seismic conversion. Rather, it agrees perfectly with the source parameters of the main aftershock (54.09°N; 163.14°W; 12:55:49.6 GMT). The latter is clearly regular in terms of source duration, as documented by its impulsive teleseismic P waves, its magnitude–moment combination ($m_b = 6.7$; $M_m = 6.4$), and the reports of the operators of the radio station at Scotch Cap, who felt it stronger than the mainshock, 22 min before flooding by the tsunami (Sanford 1946).

We therefore associate the weak T phase observed at HVO with the 12:55 aftershock rather than with the mainshock. This interpretation is supported by the detection, on the HVO record, of an even weaker T phase at 14:13, consistent with the timing of next large aftershock at 13:29 GMT. In contrast, we could find no evidence on the HVO record of any high-frequency energy around 13:11 GMT, when a mainshock T phase would have been expected. Although qualitative in nature, this observation is fundamental in the context of the present paper, since it confirms that the 1946 Aleutian earthquake, a characteristic tsunami earthquake and at $\Theta = -7.0$ the slowest event yet measured in terms of energy-to-moment ratios (Okal & Lopez 2002), did feature a strong T-wave deficiency. In this respect, the mainshock at 12:29 GMT and the main aftershock at 12:55 GMT constitute a slow–regular doublet comparable to those described above, for example the 1975–1973 events, or the 1963 aftershock–foreshock sequence, both in the Kurile Islands.
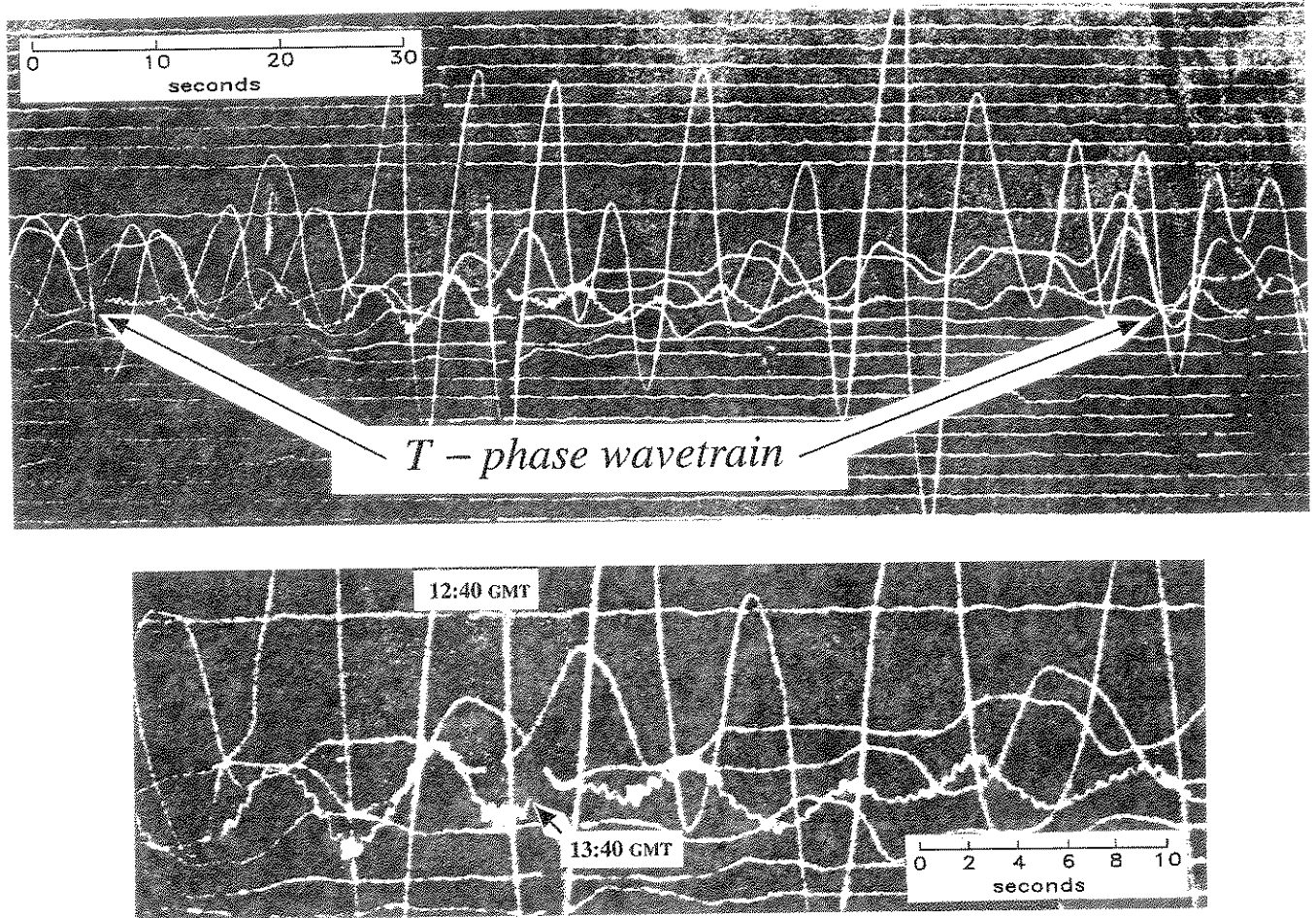
HVO — 01 APRIL 1946

Figure 8. Seismogram of the *T* phase at Hawaii Volcano Observatory following the Aleutian earthquake of 1946 April 1, photographed directly from the original smoked paper record. On the top frame, the *T* wave train appears as a wiggly phase lasting approximately 100 s. The close-up on the bottom frame allows a tentative measurement of the frequency of the signal (∼2 Hz). The upper trace of the bottom frame features the weak, low-frequency ground motion between the *P* and *S* phases of the mainshock, which verifies the time of the minute mark as 02:10 local (12:40 GMT). The *T* wave is present four traces (or 1 h) later, at 13:40 GMT, and thus it cannot be associated with the mainshock.

5 DISCUSSION

While the data set examined in this paper is arguably small, it defines a perfectly consistent trend: with no exception, all six events studied, recognized in the literature as tsunami earthquakes, feature a deficiency in *T*-phase energy flux, quantifiable for four of them through the parameter Γ at between 1.5 and 2.5 orders of magnitude. In addition to exhibiting much reduced amplitudes, the *T* wave trains of tsunami earthquakes have extended durations of up to 4 min in the case of the 1992 Nicaragua event.

This is, of course, in excellent agreement with the interpretation of tsunami earthquakes as resulting from an exceptionally slow propagation of rupture along the fault plane (e.g. Kanamori & Kikuchi 1993). Within this framework, the interference of individual elements of the source can remain constructive only at the longest periods, characteristic of mantle surface waves and tsunamis. At frequencies typical of short-period body waves (≈1 Hz), the interference is destructive, resulting in low amplitudes, m_b: M_s discrepancies and deficiencies in energy-to-moment ratios reaching typically 1–1.5 orders of magnitude (Newman & Okal 1998). At

the frequencies characteristic of propagation in the SOFAR channel ($f \geq 2.5$ Hz), the situation is simply exacerbated, with the parameter Γ being deficient by 1.5–2.5 orders of magnitude.

In his study of the 1963 and 1975 tsunami earthquakes in the Kurile Islands and Japan, Fukao (1979) had argued that their exceptional tsunamis were not necessarily caused by a prolonged source duration, but rather by rupturing inside a sedimentary wedge, where the lesser rigidity of the material would lead to enhanced strong motion at the sea floor, and hence to increased tsunami generation. Okal (1988) also showed that in certain geometries, including a standard 45°-dipping thrust fault, tsunami generation would be enhanced in low-rigidity materials, relative to surface wave excitation. However, as illustrated by Talandier & Okal (1998), a teleseismic *T*-wave train is controlled by the strong motion displacement field at the source-side conversion shore, and an increase in the amplitude of the latter should also lead to the generation of more intense *T* waves. Clearly, this is not the case for the data set of tsunami earthquakes examined in the present paper. These arguments can be reconciled if the source is exceptionally long: the tsunami generation is sensitive to the very-long period, or static, displacement

RAR (Rarotonga) -- Vertical Broadband

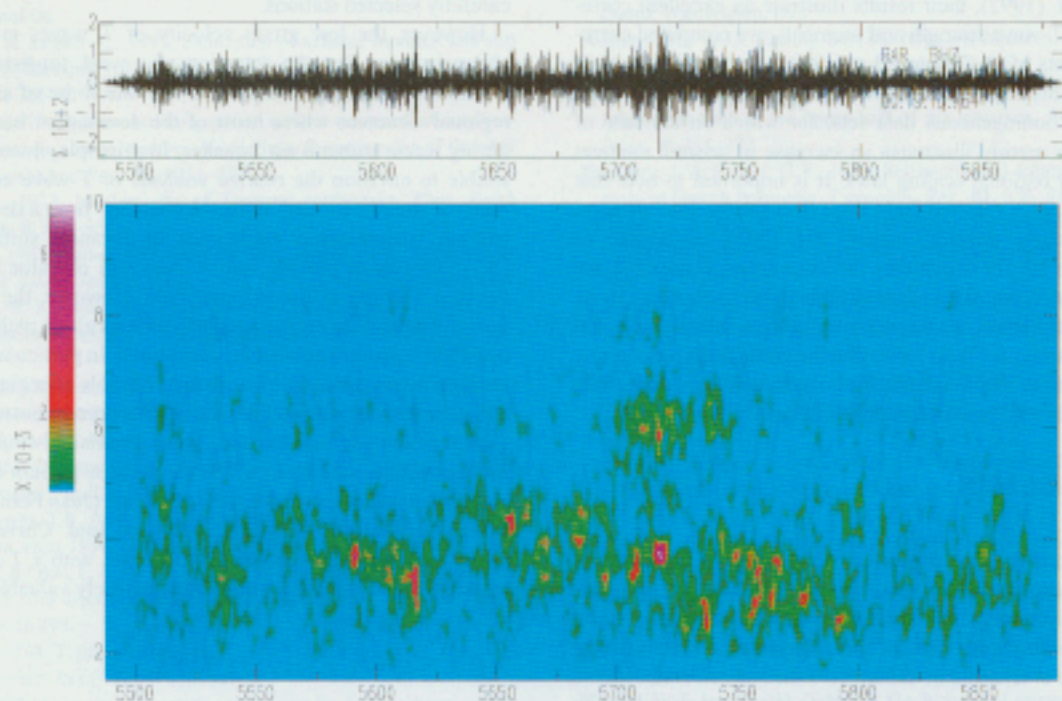## 02 SEP 1992 — NICARAGUA — Tsunami Earthquake

Figure 9. Spectrogram of the *T* phase recorded at Rarotonga from the 1992 Nicaragua tsunami earthquake. Note the long duration of the wave train, and its extremely fragmented nature, most energy puffs being separated by periods of relative quiescence, lasting as long as 20 s.

field, integrated coherently over the whole duration of the seismic release, while the *T*-phase amplitude is controlled exclusively by its very high-frequency components for which interference over a duration of many periods is essentially destructive. Our present results, including the long duration of the 1963 and 1975 *T* phases, support the model of a very slow rupture for both events, as do our determinations of the slowness parameters Θ (respectively, −6.42 and −6.43) from the Benioff 1–90 records at Pasadena.

Because of their high frequencies, *T* phases can be further used to probe into the time history of seismic sources. The spectrograms in Fig. 3 illustrate a clear difference between the two 1996 Peruvian earthquakes: whereas the Nazca *T* waves constitute an essentially continuous wavepacket lasting 100 s at a fairly constant energy level, the Chimbote wave train is considerably more scattered in time, the total duration approaching 250 s, and the level fluctuating significantly during that window. Indeed, the *T* phases consist of a succession of individual puffs, occasionally separated from each other by 5 s or more. This behaviour is also present in the 1992 Nicaragua *T* waves at RAR analysed in Fig. 9, which are shown to last ≈250 s, with short puffs of energy separated by as much as 20 s. Note, in particular, that only one puff (250 s into the window shown in Fig. 9) features high frequencies reaching above 6 Hz.

Such observations are generally consistent with the model of jerky rupture proposed for tsunami earthquakes by Tanioka *et al.* (1997) and Polet & Kanamori (2000). In this model, and for a sediment-starved environment, the fault rupture is able to propagate upwards along the plate interface; in the presence of a subducting horst-and-graben structure, the coupling of the fault walls may be laterally heterogeneous, leading to an irregular, jerky, and on the average slow, mode of strain release. The *T* waves from the Nicaragua and Chimbote tsunami earthquakes, analysed in Figs 4 and 9, strongly support this model.

On the other hand, our results for tsunami earthquakes clearly contradict the assertion by Hiyoshi *et al.* (1992), Walker *et al.* (1992) and Walker & Bernard (1993) that tsunamigenesis correlates positively with the strength of *T* phases, and this matter deserves discussion. We first note that these authors used exclusively hydrophone records, and worked at generally much higher frequencies (10–35 Hz) than us. They elected to quantify the *T* phase through the concept of 'strength' (hereafter, *S*) of the pressure signal recorded in the water, which they define as the level, measured in dB, of the amplitude spectrum of the pressure, relative to 1 μPa Hz$^{-1/2}$. We can reasonably assume that the pressure signal will scale with particle velocity through constant parameters (densities and elastic constants of water and receiving shore), so that their strength *S* and our flux TPEF must be related through an expression of form $S = S_0 + 10 \log_{10}$ TPEF. Under the assumption of seismic scaling for the source, TPEF scales linearly with the moment M_0, and we would expect *S* to vary linearly, with a slope of 10, as a function of $\log_{10} M_0$. Indeed, we have verified that the data sets presented in fig. 17 of Walker *et al.* (1992) and figs 6 and 7 of Hiyoshi *et al.* (1992) have best-regressed slopes of 13.8, 7.2 and 7.9, respectively, which can be regarded as acceptably close to 10.

Conversely, the deficiencies in Γ that we observe for tsunami earthquakes (namely factors of 30–300), would correspond to deficiencies of 15–25 dB in the parameter S. These estimates are much greater than any scatter in Walker *et al.*'s (1992) and Hiyoshi *et al.*'s (1992) data sets, where the most negative residual is −8 dB (−9 dB if the slope is forced to take a value of 10). As underscored by Walker *et al.* (1992), their results illustrate an excellent correlation between T-wave strength and moments: we computed correlation coefficients of 96, 78 and 91 per cent, respectively, for their three figures. This can be best explained by a careful selection of geographically homogeneous data sets, for which an increase of tsunami genesis merely illustrates an increase in seismic moment under global or regional scaling laws. It is important to note that Walker *et al.* (1992) rejected from their data set the lone tsunami earthquake initially selected, namely the Tonga earthquake of 1982 December 19, for which they failed to detect T waves above the noise level at Wake. While they attributed this to blockage by an unspecified island chain, we have documented in Talandier & Okal (1989) and Newman & Okal (1998) that the earthquake is definitely slow; we present in Fig. 7 qualitative but irrefutable evidence that the generation of its T waves is indeed deficient.

6 CONCLUSION AND RECOMMENDATIONS

We have documented that tsunami earthquakes, characterized by stronger near- and far-field tsunami generation than would be expected from their conventional seismic magnitudes, feature strong deficiencies in the energy flux of their T phases, as recorded by seismic stations at teleseismic distances. When scaled with seismic moment, this deficiency reaches 1.5–2.5 orders of magnitude, with respect to reference events selected in the same geographic area, but following seismic scaling laws.

Our observations generally support models published in the literature to explain the mechanism of tsunami earthquakes, namely events featuring exceptionally slow rupture velocities, caused by either propagation through low-rigidity media, such as sedimentary wedges in accretionary prisms (Fukao 1979), or, conversely, to a highly heterogeneous plate interface, along which the seismic rupture propagates in an irregular, jerky mode (Tanioka *et al.* 1997; Polet & Kanamori 2000), leading to a destructive interference of the integrated seismic displacement field at all but the lowest frequencies.

The computation of Γ from the time-series of a T phase is straightforward and could easily be automated in real time, as part of detection algorithms such as TREMORS (Reymond *et al.* 1991). It would be a simple task to evaluate Γ against a catalogue of previously analysed earthquakes in the same epicentral region, and the detection of any strong deficiency could be used to identify or confirm the occurrence of a tsunami earthquake. We are motivated in this respect by the fact that tsunami earthquakes have inflicted damage at teleseismic distances, as documented in the Marquesas Islands following the 1996 Chimbote, Peru tsunami earthquake (Heinrich *et al.* 1998): run-up in excess of 1 m was observed in Taahuku Bay, Hiva Oa, and the supply ship Aranui was rocked against its wharf and slammed on the bottom of Hakahau harbour, on the island of Ua Pou, 6600 km from the epicentre (J.-L. Candelot, pers. comm., 2000). Similarly, the 1946 tsunami was catastrophic in the far field. Within this framework, it would be desirable that the T wave train at selected island stations of the IRIS network (e.g. Rarotonga, Johnston, Christmas (Pacific Ocean), Easter, Galápagos) be made routinely available in real time following major earthquakes

in the Pacific Basin. At present, the real-time broad-brand time-series are restricted to a 10-min window following the P wave; extending its duration to 2 h at selected stations would allow the real-time, possibly automated, investigation of the parameter Γ, at what must be regarded as a negligible cost in terms of data storage and transmission if the window is extended only at a handful of carefully selected stations.

However, the low group velocity of T waves in the SOFAR channel means that the detection of a weak far-field T wave by a teleseismic station would occur too late to be of any use at the regional distances where most of the devastation has taken place during recent tsunami earthquakes. In principle, it would seem desirable to envision the routine analysis of T-wave energy flux at regional stations located along the coastline from a developing, potentially tsunamigenic, earthquake, at distances sufficiently short ($\Delta \leq 15°$) as to provide information still of value for real-time tsunami warning in the regional field. However, the whole question of the possible propagation of T phases along paths grazing the coastline is, to our knowledge, unexplored. In particular, no regional stations were operating broad-band channels at regional distances along the respective coastlines during the three recent tsunami earthquakes of the previous decade. More promising would be the few exceptional geometries in which an island is present at a relatively short, regional, distance from the shoreline (Juan Fernández, Chile; Soccorro, Mexico; Middleton, Alaska; and Christmas, Indian Ocean). The instrumentation of such sites with a T-phase station transmitting in real-time would be immensely valuable.

REFERENCES

Ben-Menahem, A. & Rosenman, M., 1972. Amplitude patterns of tsunami waves from submarine earthquakes, *J. geophys. Res.*, **77**, 3097–3128.

Boatwright, J. & Choy, G.L., 1986. Teleseismic estimates of the energy radiated by shallow earthquakes, *J. geophys. Res.*, **91**, 2095–2112.

Ekström, G. & Nettles, M., 1997. Calibration of the HGLP seismograph network and centroid-moment tensor analysis of significant earthquakes of 1976, *Phys. Earth planet. Inter.*, **101**, 219–243.

Ewing, W.M., Woollard, G.P., Vine, A.C. & Worzel, J.L., 1946. Recent results in submarine geophysics, *Geol. Soc. Am. Bull.*, **57**, 909–934.

Ewing, W.M., Tolstoy, I. & Press, F., 1950. Proposed use of the T phase in tsunami warning systems, *Bull. seism. Soc. Am.*, **40**, 53–58.

Ewing, W.M., Press, F. & Worzel, J.L., 1952. Further study of the T phase, *Bull. seism. Soc. Am.*, **42**, 37–51.

Fukao, Y., 1979. Tsunami earthquake and subduction processes near deep sea trenches, *J. geophys. Res.*, **84**, 2303–2314.

Geller, R.J., 1976. Scaling relations for earthquake source parameters and magnitudes, *Bull. seism. Soc. Am.*, **66**, 1501–1523.

Heinrich, P., Schindelé, F. & Guibourg, S., 1998. Modeling of the February 1996 Peruvian tsunami, *Geophys. Res. Lett.*, **25**, 2687–2690.

Hiyoshi, Y., Walker, D.A. & McCreery, C.S., 1992. *T*-phase data and regional tsunamigenesis in Japan, *Bull. seism. Soc. Am.*, **82**, 2213–2223.

Ihmlé, P., Gomez, J.-M., Heinrich, P. & Guibourg, S., 1998. The 1996 tsunamigenic earthquake: broadband source process, *Geophys. Res. Lett.*, **25**, 1691–1694.

Johnson, R.H., 1970. Estimating earthquake rupture length from *T* waves, in *Tsunamis in the Pacific Ocean*, pp. 253–259, ed. Adams, W.A., Univ. Hawaii, Honolulu.

Johnson, J.M. & Satake, K., 1997. Estimation of seismic moment and slip distribution of the April 1, 1946, Aleutian tsunami earthquake, *J. geophys. Res.*, **102**, 11 765–11 774.

Kanamori, H., 1970. Synthesis of long-period surface waves and its application to earthquake source studies—Kurile Islands earthquake of October 13, 1963, *J. geophys. Res.*, **75**, 5011–5027.

Kanamori, H., 1972. Mechanisms of Tsunami earthquake, *Phys. Earth planet. Inter.*, **6**, 346–359.

Kanamori, H., 1985. Non-double-couple seismic source, *Proc. XXIIIrd Gen. Assemb. Intl. Assoc. Seismol. Phys. Earth Inter.*, p. 425, Tokyo (abstract).

Kanamori, H. & Kikuchi, M., 1993. The 1992 Nicaragua earthquake: a slow earthquake associated with subducted sediments, *Nature*, **361**, 714–716.

Kikuchi, M. & Kanamori, H., 1995. Source characteristics of the 1992 Nicaragua tsunami earthquake inferred from teleseismic body waves, *Pure appl. Geophys.*, **144**, 441–453.

Leet, L.D., 1951. Discussion of 'Proposed used of the *T* phase in tsunami warning systems', *Bull. seism. Soc. Am.*, **41**, 165–167.

Levitus, S., Boyer, T.P., Antonov, J., Burgett, R. & Conkright, M.E., 1994. *World Ocean Atlas 1994*, NOAA/NESDIS, Silver Springs, MD.

Newman, A.V. & Okal, E.A., 1998. Teleseismic estimates of radiated seismic energy: the E/M_0 discriminant for tsunami earthquakes, *J. geophys. Res.*, **103**, 26 885–26 898.

Northrop, J., 1974. *T* phases from the Hawaiian earthquake of April 26, 1973, *J. geophys. Res.*, **79**, 5478–5481.

Okal, E.A., 1988. Seismic parameters controlling far-field tsunami amplitudes: a review, *Natural Hazards*, **1**, 67–96.

Okal, E.A., 2001a. *T*-phase stations for the International Monitoring System of the Comprehensive Nuclear-Test Ban Treaty: a global perspective, *Seismol. Res. Lett.*, **72**, 186–196.

Okal, E.A., 2001b. 'Detached' deep earthquakes: are they really?, *Phys. Earth planet. Inter.*, **127**, 109–143

Okal, E.A. & Lopez, A.M., 2002. New seismological results on the 1946 Aleutian earthquake, *EOS, Trans. Am. geophys. Un.*, **83**, WP64 (abstract).

Okal, E.A. & Newman, A.V., 2001. Tsunami earthquakes: the quest for a regional signal, *Phys. Earth planet. Inter.*, **124**, 45–70.

Okal, E.A. & Talandier, J., 1986. *T*-wave duration, magnitudes and seismic moment of an earthquake; application to tsunami warning, *J. Phys. Earth*, **34**, 19–42.

Okal, E.A. & Talandier, J., 1997. *T* waves from the great 1994 Bolivian deep earthquake in relation to channeling of *S* wave energy up the slab, *J. geophys. Res.*, **102**, 27 421–27 437.

Okal, E.A. & Talandier, J., 1998. Correction to '*T* waves from the great 1994 Bolivian deep earthquake in relation to channeling of *S* wave energy up the slab', *J. geophys. Res.*, **103**, 2793–2794.

Okal, E.A. *et al.*, 2002. A field survey of the 1946 Aleutian tsunami in the far field, *Seismol. Res. Lett.*, **73**, 490–503

Pelayo, A.M., 1990. Earthquake source parameters inversion using body and surface waves: applications to tsunami earthquakes and to Scotia Sea seismotectonics, *PhD Thesis*, Washington University, St Louis.

Plafker, G., Okal, E.A. & Synolakis, C.E., 2002. A new survey of the 1946 Aleutian tsunami in the near field: evidence for a large underwater landslide at Davidson Bank, *Seismol. Res. Lett.*, **73**, 259 (abstract).

Polet, Y. & Kanamori, H., 2000. Shallow subduction zone earthquakes and their tsunamigenic potential, *Geophys. J. Int.* **142**, 684–702.

Reymond, D., Hyvernaud, O. & Talandier, J., 1991. Automatic detection, location, and quantification of earthquakes: application to tsunami warning, *Pure appl. Geophys.*, **135**, 361–382.

Ruegg, J.-C. *et al.*, 1996. The $M_w = 8.1$ Antofagasta (North Chile) earthquake of July 30, 1995; first results from teleseismic and geodetic data, *Geophys. Res. Lett.*, **23**, 917–920.

Rundle, J.B., 1989. Derivation of the complete Gutenberg–Richter magnitude–frequency relation using the principle of scale invariance, *J. geophys. Res.*, **94**, 12 337–12 342.

Sanford, H.B., 1946. Log of Coast guard unit number 368, Scoth Cap DF Station, relating to the Scotch Cap light station tragedy of 1946, US Coast Guard, Washington, DC.

Scholz, C.H., 1982. Scaling laws for large earthquakes: consequences for physical models, *Bull. seism. Soc. Am.*, **72**, 1–14.

Shimazaki, K., 1975. Nemuro-Oki earthquake of June 17, 1973: a lithospheric rebound at the upper half of the interface, *Phys. Earth planet. Inter.*, **9**, 315–327.

Talandier, J. & Kuster, G.T., 1976. Seismicity and submarine volcanic activity in French Polynesia, *J. geophys. Res.*, **81**, 936–948.

Talandier, J. & Okal, E.A., 1989. An algorithm for automated tsunami warning in French Polynesia, based on mantle magnitudes, *Bull. seism. Soc. Am.*, **79**, 1177–1193.

Talandier, J. & Okal, E.A., 1998. On the mechanism of conversion of seismic waves to and from *T* waves in the vicinity of island shores, *Bull. seism. Soc. Am.*, **88**, 621–632.

Talandier, J. & Okal, E.A., 2001. Identification criteria for sources of *T* waves recorded in French Polynesia, *Pure appl. Geophys.*, **158**, 567–603.

Tanioka, Y., Ruff, L.J. & Satake, K., 1997. What controls the lateral variation of large earthquake occurrence along the Japan Trench?, *Island Arc*, **6**, 261–266.

Tsuboi, C., 1956. Earthquake energy, earthquake volume, aftershock area, and strength of the Earth's crust, *J. Phys. Earth*, **4**, 63–66.

Tsuji, Y. *et al.*, 1995. Field survey of the East Java earthquake and tsunami of June 3, 1994, *Pure appl. Geophys.*, **144**, 839–854.

Vassiliou, M.S. & Kanamori, H., 1982. The energy release in earthquakes, *Bull. seism. Soc. Am.*, **72**, 371–387.

Wadati, K. & Inouye, W., 1953. On the *T* phase of seismic waves observed in Japan, *Proc. Japan Acad.*, **29**, 47–54.

Walker, D.A. & Bernard, E.N., 1993. Comparison of *T*-phase spectra and tsunami amplitudes for tsunamigenic and other earthquakes, *J. geophys. Res.*, **98**, 12 557–12 565.

Walker, D.A. & Okubo, P.G., 1994. The *T* phase of the 1 April 1946 Aleutian Islands tsunami earthquake, *Sci. Tsunami Haz.*, **12**, 39–52.

Walker, D.A., McCreery, C.S. & Hiyoshi, Y., 1992. *T*-phase spectra, seismic moment and tsunamigenesis, *Bull. seism. Soc. Am.*, **82**, 1275–1305.

Ward, S.N., 1980. Relationships of tsunami generation and an earthquake source, *J. Phys. Earth*, **28**, 441–474.

Wessel, P. & Smith, W.H.F., 1991. Free software helps map and display data, *Eos, Trans. Am. Un.*, **72,**, 441, 445–446.

APPENDIX A: PROCESSING OF ANALOGUE DATA

Analogue data were acquired (before *ca.* 1994) at the RSP through principal short-period channels (Talandier & Kuster 1976). One was a traditional low-gain ($\approx$10 000) short-period system. The other two used a band-rejection filter peaked at 0.33 Hz to eliminate microseismic noise from sea swell: the high-gain short-period channel offered routine amplifications of $\approx$100 000 at 1 Hz, and the so-called *T*-wave channel used further high-pass filters to boost magnification in the seismoacoustic band (2–10 Hz) to as much as 2×10^6 at 3 Hz (Okal 2001a).

As discussed in Talandier & Okal (2001), we have found it possible to digitize paper records from the RSP (with a paper speed of 15–18 cm min^{-1}), at a sample rate of 10 Hz (occasionally 20 Hz), after enlarging them fourfold on a photocopier. The resulting time-series thus have a Nyquist frequency $f_N = 5$ Hz, and can provide valuable spectral information in the 2–5 Hz range.
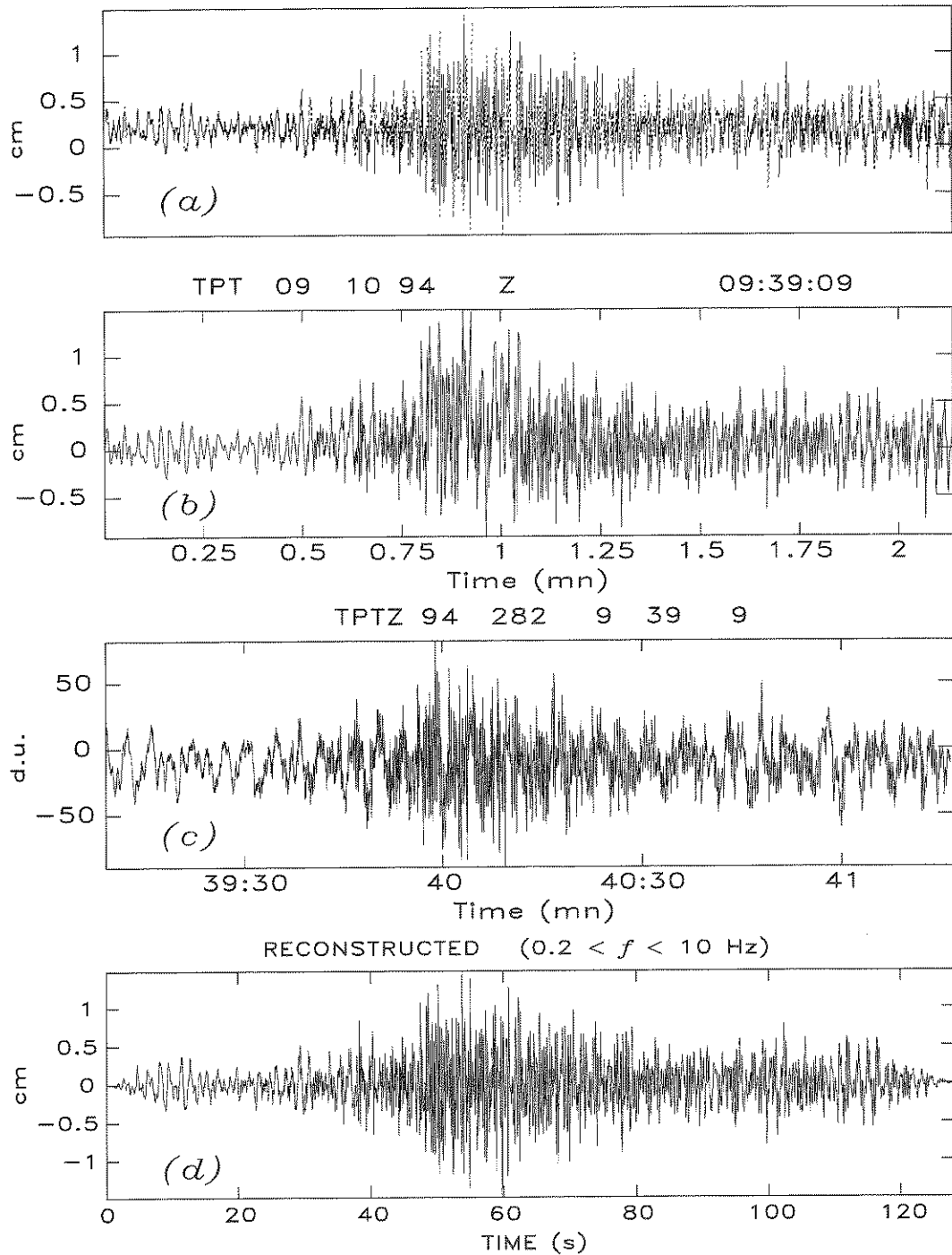
Figure A1. Comparison of records obtained at TPT (Tiputa, Rangiroa) of the *T* phase from the Kurile Islands earthquake of 1994 October 9 (origin time 07:55:40 GMT). All traces are 128 s long, and start at 09:39:09. (a) Original paper record as written on the high-gain short-period channel, featuring a magnification of 125 000 at 1 Hz. (b) Digitized version of the paper record, sampled at 10 Hz. (c) Plot of the corresponding seismogram, as recorded digitally. (d) 'Analogue' record reconstructed from the digital trace by deconvolving the response of the digital system, and applying that of the analogue recorder, in the frequency band 0.5–10 Hz.

Because of a loss of contribution to the integral (2) between ω_N and ω_{max}, it becomes impossible to directly compare expressions of TPEF from analogue and digital records. In addition, there remains some uncertainty as to the reliability of the method at the higher-frequency end of the spectrum. To alleviate these problems, we compare values obtained from paper and digital records of the same wave train (same event at the same station), using the *T* phase recorded at Tiputa (TPT) from the earthquake of 1994 October 9 (Origin Time 07:55 GMT) in the Kurile Islands, at a time when both analogue and digital systems were in operation. Fig. A1 shows the original paper record (a) and its digitized version (b), and compares them with the digital record (c). After removing the

Table A1. Comparison of results from digital and analogue records for the Kuriles event of 1994 October 9.

Event	Distance (deg)	Backazimuth (deg)	Moment (10^{20} N m)	Duration of time window processed (s)	Frequency band f_{min} (Hz)	f_{max} (Hz)	TPEF (kg s^{-2})	Γ (m^{-2})	Ratio to previous entry
				Station: Tiputa (TPT)					
94282 Kuriles (paper)	82.99	319	0.94	150	2	5	2.97×10^{-6}	3.16×10^{-26}	
94282 Kuriles (Digital)	82.99	319	0.94	150	2	5	7.94×10^{-6}	8.44×10^{-26}	2.6
				Station: Pomariorio (PMO)					
94282 Kuriles (Digital)	82.84	319	0.94	150	2	5	2.03×10^{-4}	2.16×10^{24}	25.6
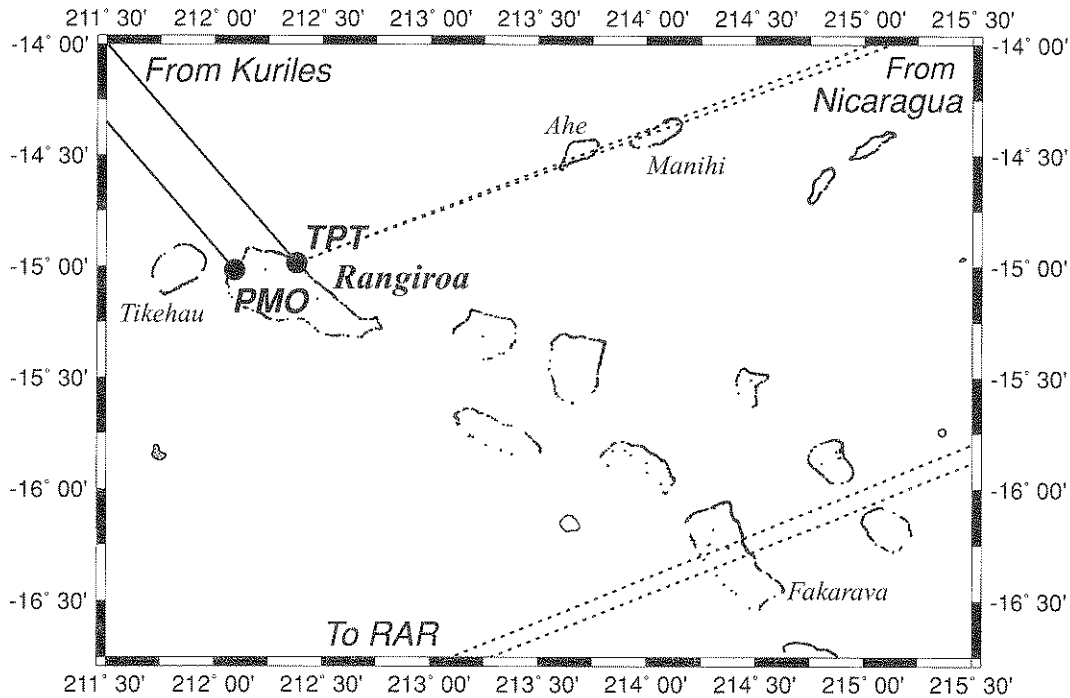
Figure A2. Map of the northwestern Tuamotu Islands, showing the atoll of Rangiroa, with stations PMO and TPT (solid dots). The solid lines are the great circle paths from the 1994 Kuriles event to PMO and TPT. The dashed lines show the great circle paths from the Nicaraguan events to station TPT, intersecting the atolls of Manihi and Ahe. To the Southeast, the map shows the great circle paths to RAR intersecting Fakarava.

transfer function of the analogue system, we compute a value TPEF$_{paper}$ = 2.97×10^{-6} kg s^{-2}, which can be compared with the flux TPEF$_{dig}$ = 7.94×10^{-6} kg s^{-2}, from the digital record, the upper bound of the integration being restricted to f_N = 5 Hz. The ratio of these two estimates, 2.67, or 0.43 logarithmic units in energy (0.21 unit in amplitude) expresses the obvious limitations of the method, and can be regarded as an empirical correction to be applied to estimates of TPEF, and hence of Γ, obtained from paper records (Table A1).

Another problem arises from the limited dynamic range of the paper records, which results in frequent saturation (e.g. Fig. 7). We overcome this difficulty by using on-scale records at a station involving a less favourable conversion, such as TPT in the case of epicentres in the Kurile Islands (Fig. A2). Again using the modern reference event of 1994 October 9, recorded digitally at both stations, we find an energy flux at PMO, TPEF$_{PMO}$ = 2.03×10^{-4} kg s^{-2}, which is R = 25.6 = $10^{1.41}$ times greater than at TPT. This illustrates the poor conversion, under nearly grazing incidence, at TPT, or even possibly the fall-off with distance of the energy in the T phase, which has propagated seismically across the atoll on a path from PMO to TPT, suffering anelastic attenuation along the way. R can then be used as an empirical correction to estimate TPEF$_{PMO}$ for saturated paper records of other events in the Kuriles, using unclipped traces at TPT.